Advanced Steel Construction – Vol. 21 No. 5 (2025) 425–435
DOI:10.18057/IJASC.2025.21.5.5

LOAD-SLIP BEHAVIOR OF PERFOBOND SHEAR CONNECTORS POST HYDROCHLORIC ACID CORROSION ON BEARING CAPACITY

Fan Yang [1], Wen-Jing Qiao [1,*], Ting-Kun Zhou [1], Yun-Long Li [1], Zhi-Dan Ruan [1] and Shou-Fu Li [2]

[1] *Dept. of Civil and Architecture Engineering, Xi'an Technological Univ., Xuefuzhonglu Ave., Weiyang District, Xi'an City, Shaanxi Province 710021, China*
[2] *China Construction Third Bureau Group Northwest Limited company, Jinyelu Ave., Yanta District, Xi'an City, Shaanxi Province 710076, China*
** (Corresponding author: E-mail: qiaowenjing@xatu.edu.cn)*

ABSTRACT

The study conducted push-out tests on seven specimen groups to investigate the load-slip behavior of PBL shear connectors affected by hydrochloric acid corrosion. Among them, the corrosion time of PBL shear connectors in specimens was 0, 1, 4, 12, 24, 48 and 72 h, respectively. Based on the test verification, 147 refined finite element models with varying corrosion durations were developed to examine factors such as concrete strength grade, end bearing conditions, penetrated steel bar diameter, and hole size in the steel plate. The load-slip characteristics decrease gradually with increased corrosion time. When the concrete grade, penetrated steel bar diameter, and steel plate hole size were increased to C60, 25 mm, and 65 mm, the slippage decreased by 17.13%, 9.49%, and 11.77%, respectively. Additionally, the slip amount under end pressure was 8.26% lower compared to that without end pressure. The load-slip formula is proposed by comparing the test findings.

ARTICLE HISTORY

Received: 22 July 2024
Revised: 15 January 2025
Accepted: 6 February 2025

KEYWORDS

Perfobond shear connectors;
Hydrochloric acid corrosion;
Push-out experiment;
Load-slip characteristics

1. Introduction

PBL shear connectors enable the concrete to constrain the steel beam's compression flange, thereby improving its stability [1-4]. Meanwhile, tanks carrying dangerous chemicals are increasing day by day. When the corrosive liquid in the vehicle overturns and penetrates penetrated steel bar. This action can lead to the corrosion of shear connectors to diminish their load-slip behaviour. Therefore, ductility and durability of the bridge decrease. Hence, it is urgent for PBL shear connectors to study the load-slip behaviour with hydrochloric acid corrosion.

At present, load slip properties and fatigue propertiesof PBL shear connectors have been studied extensively [5-6]. Yang took the numerical regression analysis method to establish the load-slip curve [7]. Xiao analyzed the load transfer characteristics, load slip law and mechanical properties [8]. Aguiar failure mode, controlled by transverse reinforcement, proposed an innovative model to forecast the entire load-slip curve [9]. Le proposed an efficient long short-term memory-based model for prediction of the load-displacement curve of concrete-filled double-skin steel tubular columns[10]. While the experimental and numerical investigations provide the load-slip curve[11-13], a calculation formula still needs to be established.

It is well known that different stages of load-slip curves are in various forms. Li put forward linear and power law models of elastic and elastoplastic stages [14]; Wang also raised linear and log models of the same stages [15]. Cao JX predicted the nonlinear behaviour based on load-slip curves of composite materials and used a Bayesian method to quantify model parameters [16]. Huang selected two introduced position functions to establish the relative slip constitutive model [17]. Cao YM posed a descriptive model of shear slip characteristics taking into the stiffness of elastic connectors of connectors account [18]. In view of the above mathematical models of the load-slip formula, scholars also studied the effects of various factors on load-slip, including ultra-high performance, ordinary, lightweight, high-strength and lightweight high-strength concrete; bond friction between transverse reinforcement and elliptical holes; round and long holes of the connectors [19-23]. However, the load-slip behavior of shear link components in a hydrochloric acid environment was not considered in the above research.

To summarize, prior research has been dedicated to investigating the impact of atmospheric exposure on the mechanical performance of PBL shear connectors, with a focus on developing formulas specific to atmospheric corrosion conditions. The research primarily concentrated on the mechanical behavior of PBL shear connectors and the influence of parameters such as the thickness of perforated steel plates, the size of the openings, the strength grade of the concrete, and the diameter of the through-reinforcement. When 36% industrial hydrochloric acid contact penetrates the steel bar in a short time, the strong-corrosion will affect the overall durability of the composite structure. This paper examines the load-slip behavior and formula of PBL shear link components corroded by industrial hydrochloric acid, based on push-out tests and finite element modeling (FEM). The findings establish a foundation for analyzing the structural and mechanical properties following strong acid corrosion.

2. Experimental setup

2.1. Design of test specimens

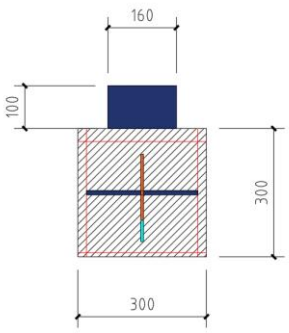

(a)Axonometric drawing

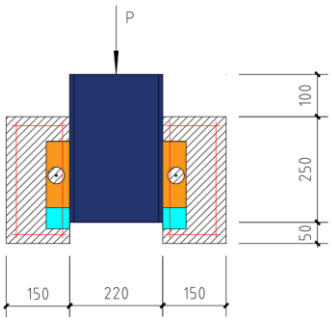

(b)Main view

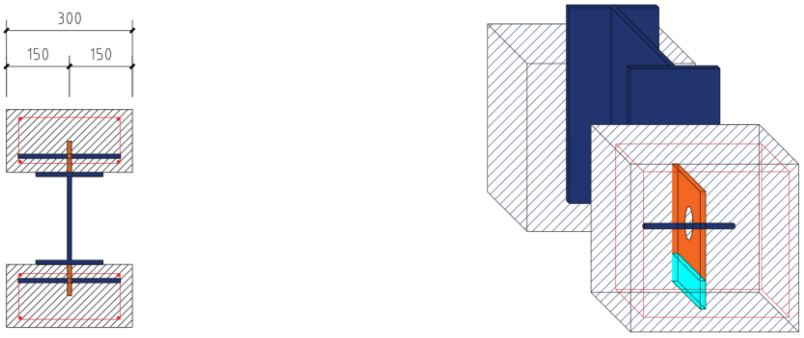

(c)Side view (d)3D view

Fig. 1 Specimen structure (Units: mm)

The design included fourteen specimens arranged into seven groups. The main parameter sizes are shown in Fig. 1. The specimen mainly comprises C50 concrete, φ10mm HPB300 light round steel bar of ordinary steel bars, and φ14 HRB400 screwed reinforcement. According to the above data, the reinforcement rate of the specimen is 0.60% transverse and 0.69% longitudinal. In addition, both I-steel and perforated steel plate are Q345q；the size is I-steel 220mm×160mm×16mm×16mm, and perforated steel plate 160mm×80mm ×16mm.

The penetrated steel bar was corroded 0, 1, 4, 12, 24, 48 and 72 h, respectively. Then, the loss rate with different corrosion times was measured. The tensile test, conducted using the CSS-44000 series electronic universal testing machine, determined the mechanical properties, including elongation and strength. The rate of loading is elastic stage 0.75 mm/min, and yield stage 5 mm/min. The test procedure strictly adhered to the stipulations of GB/T 228.1-2021, "Test Method for Metal Tensile Properties"[24]. Table 1 indicated the penetrated steel bars' material mechanical indexes.

Table 1
The penetrated steel bars' material mechanics index with different corrosion time

Corrosion time/h	Corrosion rate/%	Ultimate strength/MPa	Yield strength/MPa	Elasticity modulus/Gpa
	0.00	573.78	423.44	218.58
0	0.00	578.47	390.67	220.91
	0.00	586.02	388.97	217.61
	0.54	571.69	396.00	217.34
1	0.49	578.94	402.72	218.43
	0.46	578.68	402.56	213.34
	1.75	601.03	391.00	208.96
4	1.83	555.53	396.00	211.89
	1.80	556.60	403.00	210.83
	3.28	548.57	393.00	206.76
12	3.28	546.35	390.00	203.78
	3.35	597.25	392.00	200.74
	6.67	552.82	385.99	202.55
24	5.98	556.11	389.39	198.77
	4.36	560.40	392.73	200.69
	5.55	552.82	387.00	198.79
48	6.22	556.11	383.00	197.63
	7.80	560.40	381.00	191.97
	9.10	553.20	382.00	190.68
72	9.25	552.49	382.00	193.47
	9.47	551.67	383.00	193.14

2.2. Test procedure

The test adopted a 2000 kN hydraulic four-column pressure testing machine (see Fig. 2). The loading method was firstly preloading the specimen at 80 kN for 3 times. The formal loading rate was adjusted to 1kN/s, and then the specimens were yielded at 10% the estimated ultimate load. During the 2 min load holding stage of each stage, the load displacement of equipment and the cracks of the specimens were needed to record. Subsequently, the loading was stopped when the bearing capacity decreased to 70% of the ultimate load, with increments of 1 mm.

Fig. 2 Test arrangement and instrumentation

3. Experimental results

3.1. Test phenomena

The load on the I-steel transferred to the concrete plate at the beginning of loading. It can be seen that the bottom of the concrete plate has a small part of the concrete to produce many tiny cracks. At 0.69 Pu (ultimate load), the concrete on the contact surface between the concrete slab and the I-beam starts to detach, accompanied by a faint sound. As the loading reaches 0.82 Pu, small cracks begin to form in the center and along the bottom edge of the concrete slab, indicating that the sample is approaching the yield stage. The cracks are about 0.05 mm in width and 4~5 cm in length. After that, if the specimen arrived at peak bearing capacity, the sound inside makes a rattling sound, and 45° oblique cracks appear inside the concrete slab, extending to the periphery with a length of up to 6~7 cm. The cracks of the specimen mainly appear on the outside and inside surfaces of the concrete. Fig. 3 explains failure forms of specimens.

After corroded PBL shear link components are shear, the bending angles of the penetrated steel bar are 7.8°, 9.5°, 13.0°, 14.9°, 18.5°, 19.7°, and 21.1°, respectively (Fig. 4). At the same time, concrete cracks are deepened and lengthened. The initial crack load at corrosion time is 306.16, 287.22, 270.35, 268.33, 264.08, 251.67, and 231.26 kN, respectively. Additionally, The maximum bearing capacity with a 45° inclined crack decreases to 332.30, 311.74, 293.42, 291.24, 286.62, 273.16, 251.00 kN in turn.

(a) Front (b) Back

(c) Facies medialis (d) Top

Fig. 3 Failure mode

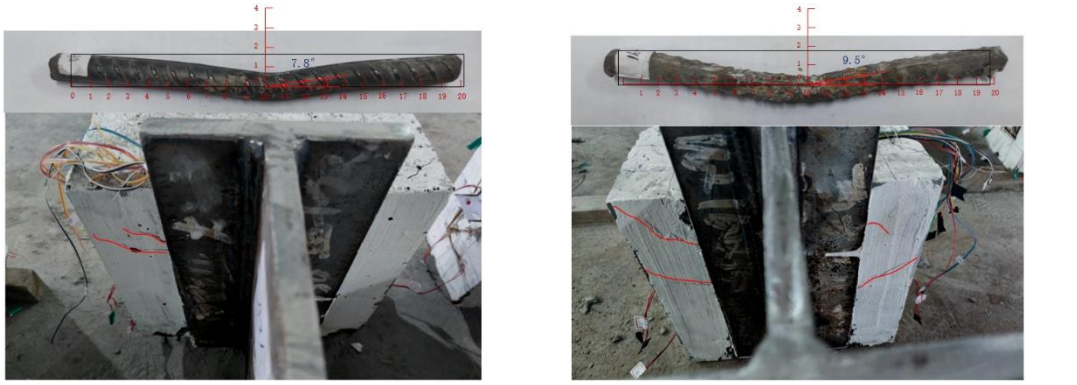

(a) 0 h (b) 1 h

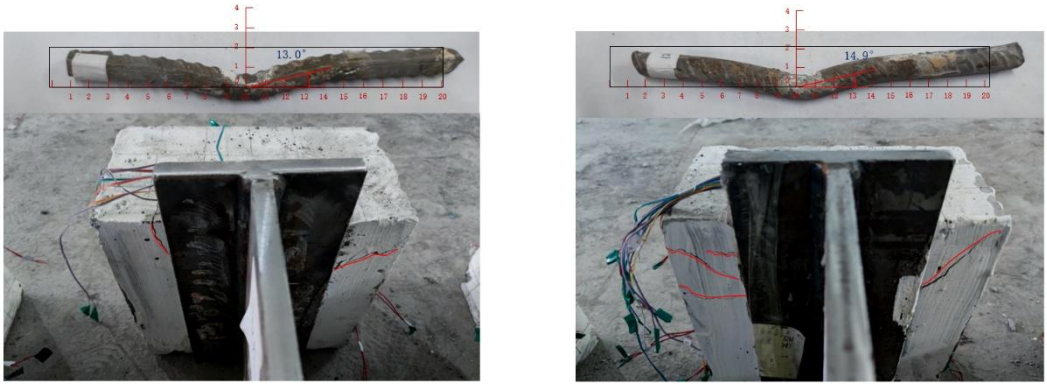

(c) 4 h (d) 12 h

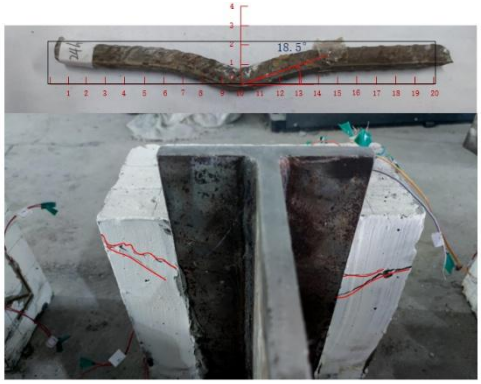

(e) 24 h

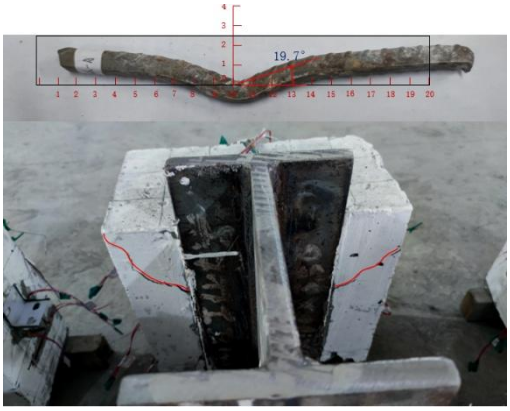

(f) 48 h

(g) 72 h

Fig. 4 Failure modes of corroded specimens

3.2. Load-slip curves

In evaluating the mechanical properties, the load-slip curve in Fig. 5 illustrates the relative deformation of steel and concrete as the load varies. It highlights the three key mechanical characteristics: ultimate bearing capacity, shear stiffness, and deformability of the shear link components. The data characteristic points of the curve are demonstrated in Table 2.

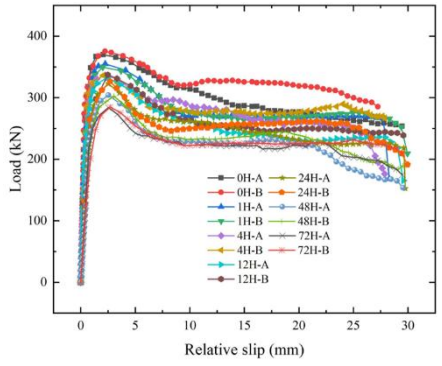

Fig. 5 Load-slip curves

In table 2, the maximum bearing capacity Pu decreases by 0%, 3.76%, 6.33%, 9.54%, 13.86%, 17.91%, and 24.57%, respectively; the relative slip amount δ_u increased by 0%, 4.43%, 14.78%, 19.21%, 23.64%, 32.02%, and 34.48%, respectively; the ultimate slip amount δuk decreased by 0%, 4.75%, 8.86%, 10.82%, 35.43%, 42.14%, and 59.25%, respectively; shear stiffness k_s decreased by 0%, 1.56%, 2.69%, 3.77%, 5.22%, 6.37%, and 9.17%, respectively; ductility coefficient δ_{uk}/δ_{rk} decreased by 0%, 29.55%, 39.92%, 46.65%, 63.46%, 70.03%, and 77.41%, respectively. A contributing factor to the decline in mechanical properties is the decrease in the diameter of the penetrated steel bar.

Table 2
The data characteristic points of the curve in the test

Corrosion time/h	Bearing capacity P_u/kN	Peak slip δ_u/mm	P_{rk}=0.9P_u/kN	δ_{rk}/mm	Ultimate slip δ_{uk}	Shear stiffness K_s/kN·mm	Ductility factor δ_{uk}/δ_{rk}
0	378.83	1.96	341.23	1.24	8.74	494.23	6.42
	367.93	2.1	330.85	0.88	8.46	483.99	6.24
1	363.84	2.09	323.67	1.43	8.44	486.34	5.14
	336.7	2.15	306.81	1.39	7.98	476.58	3.78
4	340.53	2.24	304.67	1.57	8.13	479.82	3.91
	318.85	2.42	288.77	1.65	7.67	472.08	3.69
12	332.87	2.38	299.85	1.64	7.91	472.98	3.65
	321.61	2.46	289.17	1.78	7.61	468.4	3.11
24	327.65	2.46	292.32	1.94	6.52	466.53	2.42
	316.45	2.56	287.38	1.84	6.18	460.61	2.2
48	313.76	2.59	282.54	1.98	6.34	460.54	2.29
	300.08	2.77	269.92	2.3	5.76	455.38	1.51
72	298.64	2.66	270.45	2.43	5.54	447.32	1.89
	265.4	2.8	237.19	2.33	5.26	441.16	0.97

Note: δ_{rk} is the slip amount of the load rising to P_{rk}; δ_{uk} is the slip amount of the maximum load descending to P_{rk}.

3.3. Load-strain curve

Load-strain curves in Fig. 6 shows the internal stress state and yield of shear link components. These data in Fig. 6 was collected by the upper and lower of penetrated steel bars.

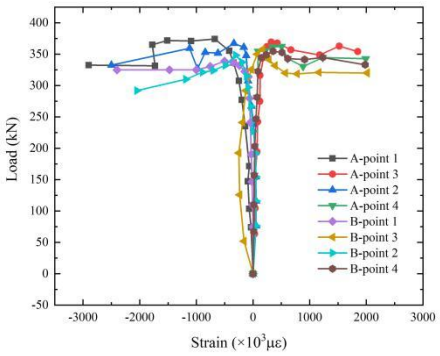

(a) 0 h

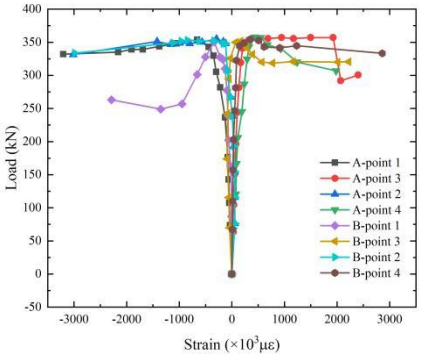

(b) 1 h

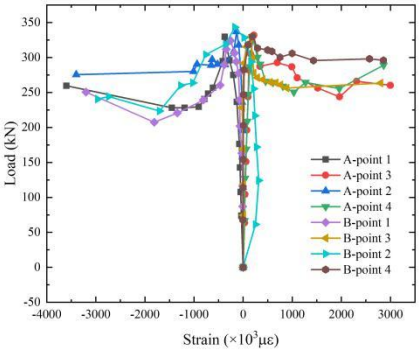

(c) 4 h

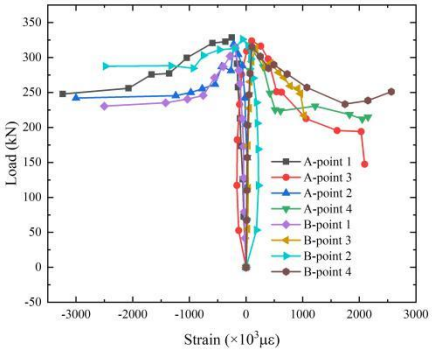

(d) 12 h

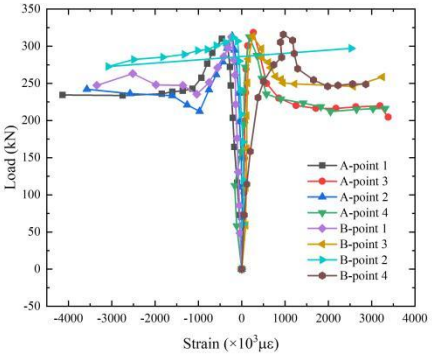

(e) 24 h

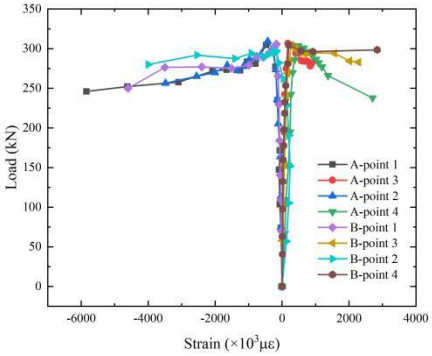

(f) 48 h

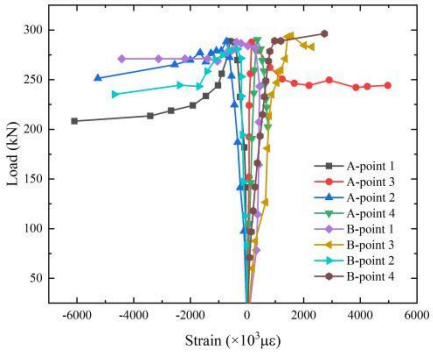

(g) 72 h

Fig. 6 Load-strain curves

As shown in Fig. 6, the compressive strain increases from -2200 με to -5300 με, while the tensile strain increases from 2000 με to 4232 με. Furthermore, at the beginning of loading stage, the strain rises slowly with the load increase. Once the steel bar reaches its yield point, the load starts to decrease, and the strain rises rapidly. The strain law is basically the same. Furthermore, the compressive strain of measuring points 1 and 2 is negative, and the tensile strain of points 3 and 4 is positive. The steel bar is in a compression-bending stress state, as its compressive strain is always greater than the tensile strain. The one-side strain value obtained from the penetrated steel bar on both sides of A and B is always greater than the other. The main reason is that the specimen will produce eccentricity with compression, resulting in a large force on one side and a small one on the other.

4. Finite element models

4.1. Finite element simulation

In order to further study the internal failure mechanism of PBL connectors during loading, the software ABAQUS was especially used to simulate tests. C3DR8 reduced solid element could simulate I-steel, perforated steel plat, concrete, and penetrated steel bar. The T3D2 was used to simulate a stirrup. Constraints were applied to bind the concrete tenon with the slab, the concrete tenon with the penetrated steel bar, and the perforated steel plate with the I-beam. The tangent line adopted the function of friction coefficient 0.904. The stirrup and concrete were linked with embedding constraints, symmetric constraints were applied at the center of the steel beam web, and fully fixed constraints were used for the concrete bottom plate. The displacement was imposed on the coupling point to simulate the loading state in Fig. 7.

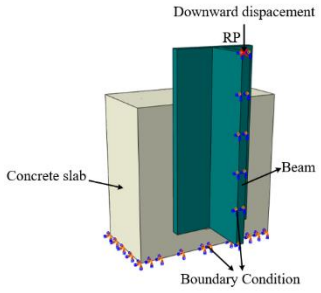

Fig. 7 1/2 model

The mesh of the FEM is fitted with 5 mm concrete tenons, 3 mm penetrating steel and 15 mm stirrups(see Fig. 8). C50 concrete use the plastic damage model with an expansion angle 30°, an eccentricity rate 0.1, and the viscosity coefficient 0.0005. Additionally, the biaxial compressive strength is 1.16 times the uniaxial compressive strength, and the constant stress ratio of the tensile meridian to the compressive meridian (K) is 2/3.The elastic modulus is 34.523 GPa, and compressive strength is 53.35 MPa, respectively. The steel exhibits a yield strength of 476.26 MPa, an ultimate strength of 613.61 MPa, an elastic modulus of 234.96 GPa, and an elongation of 43.30%.

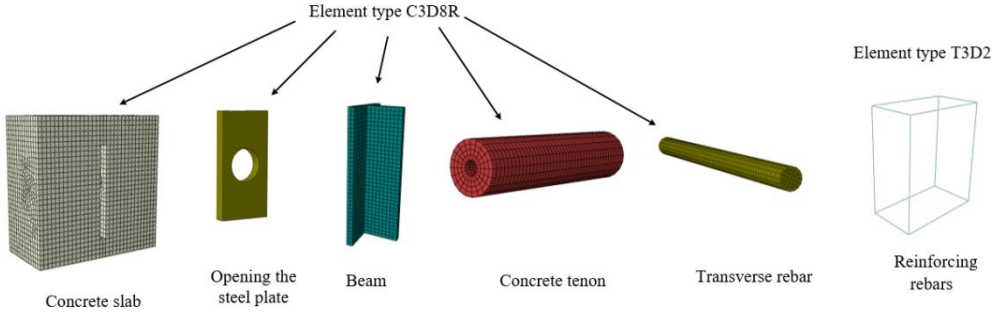

Fig. 8 Mesh generation

4.2. Finite element results and analysis

Fig. 9 shows that the test values are largely consistent with the finite element values in both the linear elastic and nonlinear stages. At ultimate shear capacity, the steel reaches its yield strength, and then the load-slip curve slip velocity increases with the increasing load. At this stage, there is a slight difference between the test and the FEM. The error is less than 10%, mainly caused by the construction error. It can be concluded from Fig. 11 that the maximum stress position is welding joint between the I-beam and perforated steel plate, so does the concrete tenon. Fig. 11 indicates that the FEM can accurately simulate the load-slip curve.

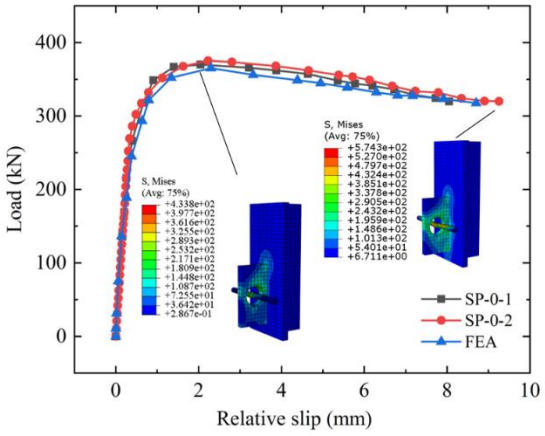

(a) 0 h

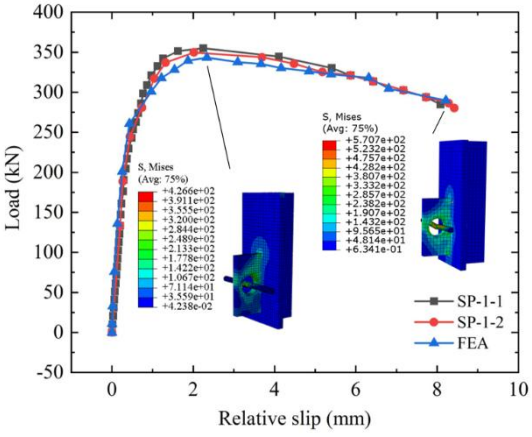

(b) 1 h

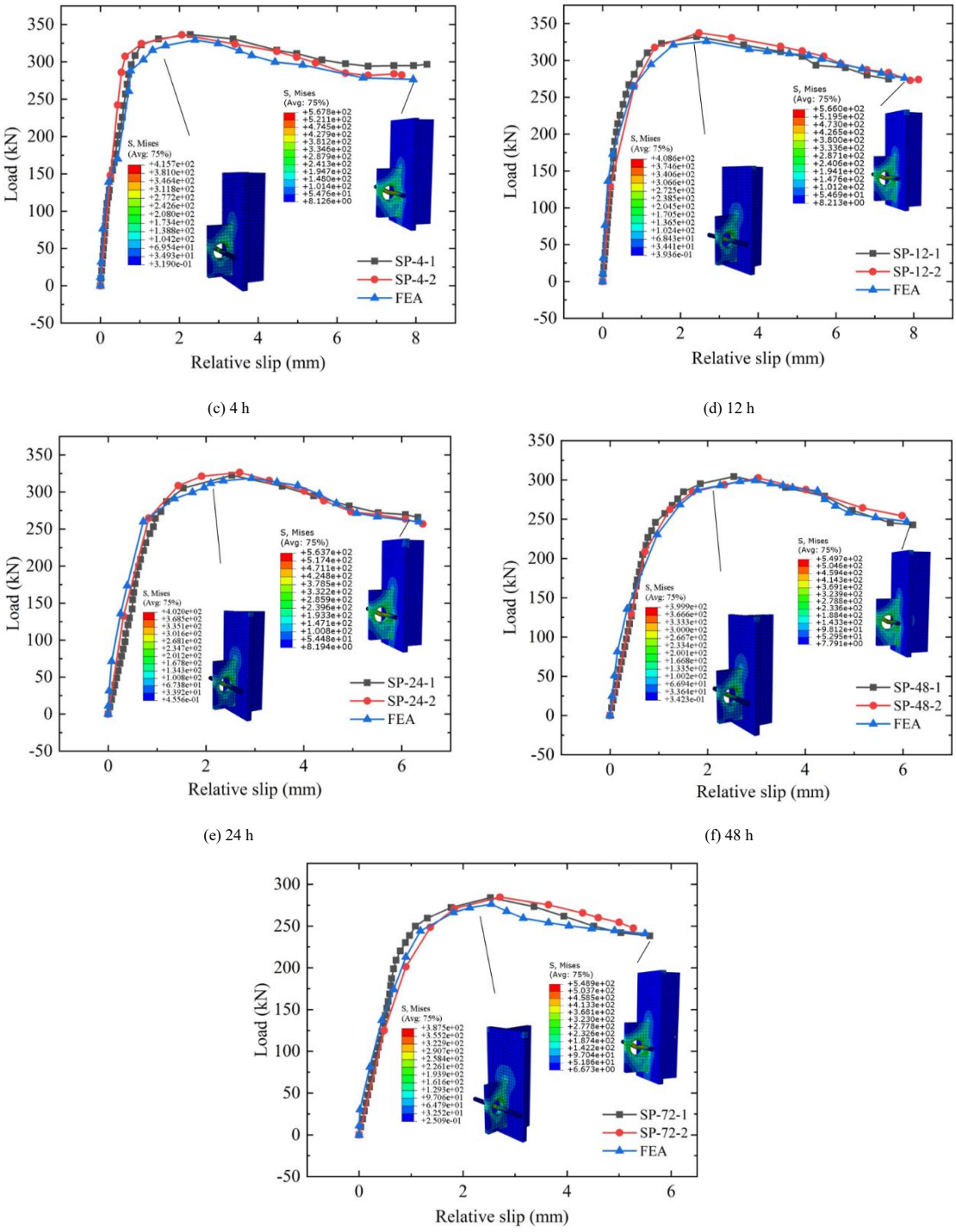

(c) 4 h

(d) 12 h

(e) 24 h

(f) 48 h

(g) 72 h

Fig. 9 Load-strain curves

4.2.1. Parametrical investigations

This paper employs software to investigate how various factors affect the shear strength and deformation under hydrochloric acid corrosion.

(1) Concrete strength. For concrete grades C30, C35, C40, C45, C50, C55, and C60, the shear bearing capacity decreased by 28.11%, 27.47%, 27.56%, 25.23%, 24.52%, 23.66%, and 22.92% as the corrosion time increased, respectively (Fig. 10(a)). Meanwhile, the slip amount decreased by 41.91%, 39.64%, 38.20%, 37.85%, 35.67%, 30.24%, and 24.78%, respectively (Fig. 11(a)).

(2) The diameter of Penetrated steel bar. For steel bars with diameters of 12mm, 14mm, 16mm, 20mm, and 25mm, the shear capacity decreased by 22.35%, 24.46%, 17.97%, 14.40%, and 12.76%, respectively (Fig. 10(b)), while the slippage reduced by 34.75%, 33.72%, 31.46%, 30.11%, and 25.26%, respectively (Fig. 11(b)).

(3) End-bearing mode. Of the non-endbearing structure, the shear capacity and the slippage are reduced by 24.47% and 33.72%. The end-bearing structure exhibited reductions of 11.16% in shear capacity and 25.46% in slippage (Fig. 10(c) and Fig. 11(c)), indicating superior anti-corrosion performance compared to the non-end bearing structure.

(4) The diameter of the steel plate holes. With an increase in diameter, the shear capacity experienced reductions of 20.35%, 20.70%, 19.75%, 19.28%, 18.44%, 17.57%, and 17.87%, respectively (Fig. 10(d)). Correspondingly, the slippage decreased by 39.80%, 35.23%, 34.35%, 33.57%, 33.72%, 32.50%, 29.28%, and 28.03%, respectively (Fig. 11(d)).

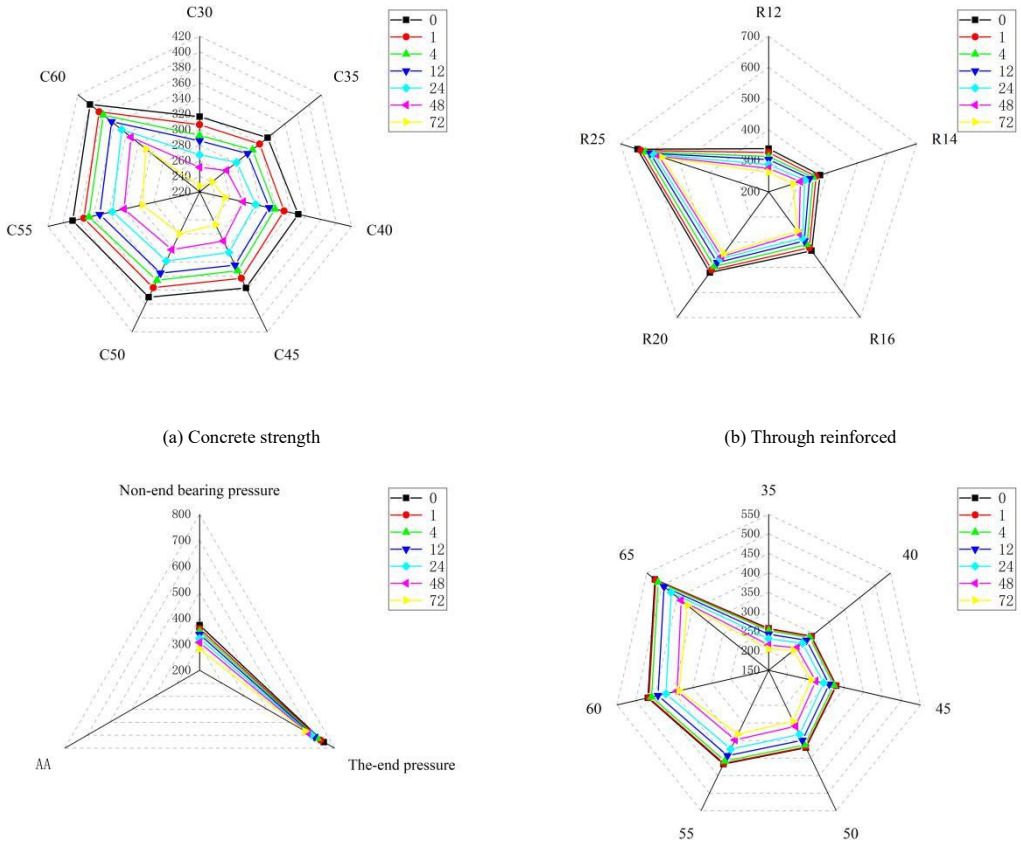

(a) Concrete strength (b) Through reinforced

(c) End bearing mode (d) Aperture of open plate

Fig. 10 Influence factors of the shear capacity

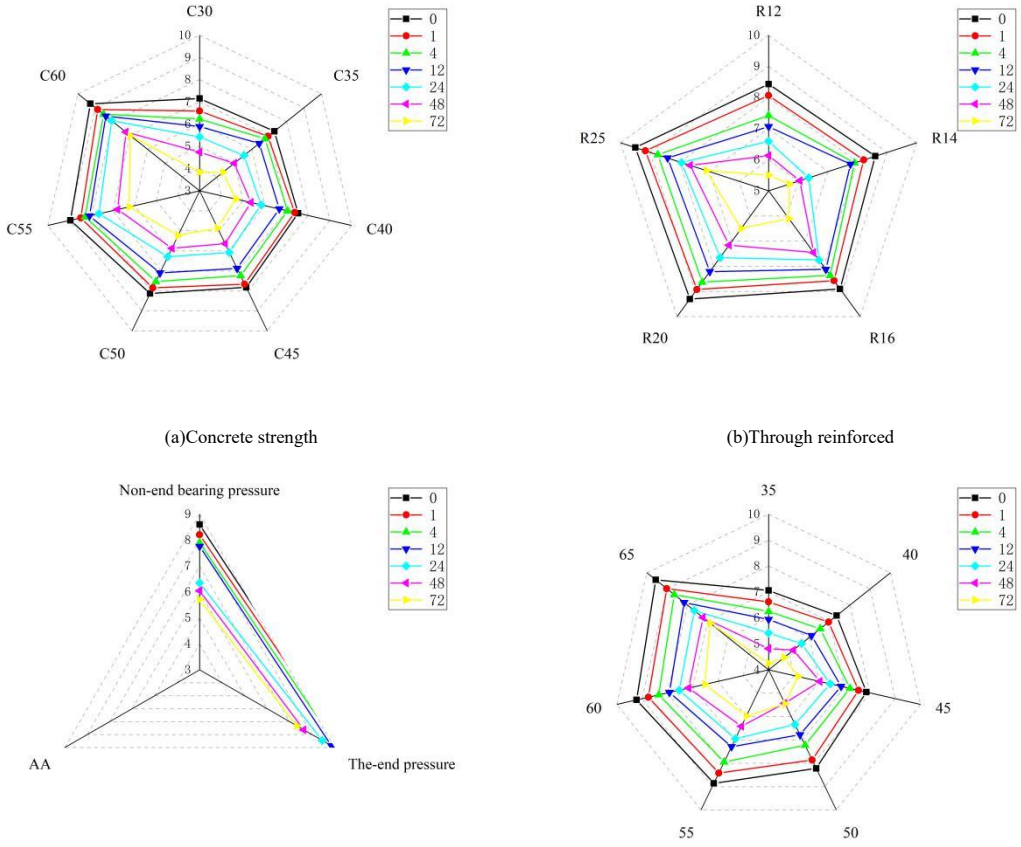

(a)Concrete strength (b)Through reinforced

(c)End bearing mode (d)Aperture of open plate

Fig. 11 Influence factors of the amount of slip of the connector

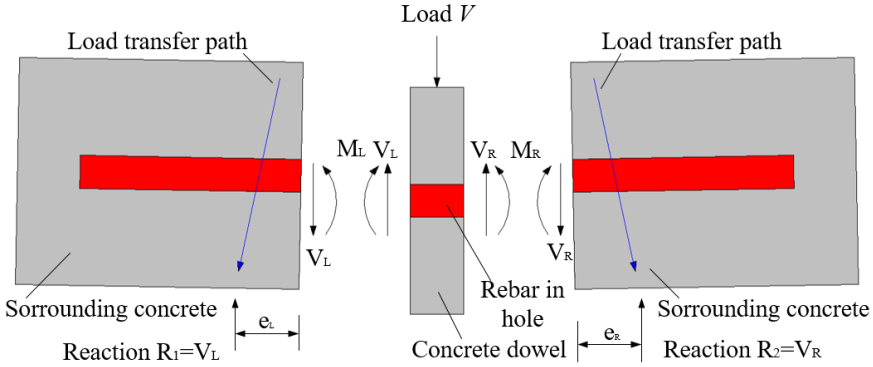

Fig. 12 The connectors' shear mechanism

5. Stud load-slip curve calculation method

5.1. Perfobond shear connector force mechanism

The shear mechanism of connectors is studied according to the test, as shown in Fig. 12. The load transfer mode at the concrete transfer bar was described, and the shear mechanism of the perforated steel bar shear connector was discussed. When Load V was applied to I-beams, I-beams transmitted shear to perforated steel plates, which in turn transmitted shear to concrete tenons and perforated steel bars. The shear and bending deformations increased the slippage S between the tenon and the surrounding concrete, producing shear VL, VR and moment ML, MR. The resistance of ML and MR was increased by the steel bar in the hole, leading to more shear and bending deformation, which in turn resulted in greater slippage between the steel bar and concrete. In Fig. 12, the load transfer extends outwards at a certain angle. As corrosion time increases, the shear link components VL, VR, ML, and MR, along with the yield strength of the steel bars, decrease, resulting in a reduction in the shear capacity of the composite structure.

5.2. Load-slip curve calculation formula

To sum up, the load-slip trend of each steel-concrete composite structure was roughly the same, including three stages: linear elastic, non-linear elastic development, and load decline stages. This paper analyzed the curves of the plastic and the descending sections. It was found that the load-slip curves could be described theoretically by a logarithmic function. Hence, the curves of the plastic and descending stages are fitted as Eq. (1):

$$\frac{P}{P_u} = a\ln(s) + b \tag{1}$$

Where, both a and b are parameters, P_u stands for the ultimate bearing capacity, and S represents the relative slip.

The origin software was used to fit the plastic and descending sections of Eq. (1) to obtain the plastic section a=0.250, b=0.915, and R^2=0.96, descending section a=-0.071,b=1.057, and R^2=0.92. Eq. (2) can be received by putting the fitting parameters a and b into Eq. (1).

$$\frac{P}{P_u} = \begin{cases} 0.250\ln(S) + 0.915 & S_i \le S \le S_p \\ -0.071\ln(S) + 1.057 & S_p \le S \end{cases} \tag{2}$$

Where, S_i denotes the initial sliding value, roughly 0.2 mm; S_p refers to the peak slip amount, and S_u represents the ultimate slip value.

The test model of linear elasticity stiffness K_s in the rising stage is formula (3).

$$K_s = \frac{P}{S} \tag{3}$$

The load-slip is shown as Eq. (4).

$$\frac{P}{P_u} = \begin{cases} \dfrac{K_S S}{P_u} & 0 \le S \le S_i \\ 0.250\ln(S) + 0.915 & S_i \le S \le S_p \\ -0.071\ln(S) + 1.057 & S_p \le S \end{cases} \tag{4}$$

5.3. Calculation formula of perfobond shear connector load-slip curve

The hydrochloric acid corrosion time t of PBL shear link components is introduced into the formula (4) to obtain the calculation model, as shown in Formula (5).

$$\frac{P}{P_u(t)} = \begin{cases} \dfrac{K_S(t) S}{P_u(t)} & 0 \le S \le S_i \\ 0.250\ln(S) + 0.915 & S_i \le S \le S_p(t) \\ -0.071\ln(S) + 1.057 & S \le S_u(t) \end{cases} \tag{5}$$

Where,

$$K_S(t) = \left(0.90 - 0.09 \times 0.96^t\right)\left(0.27 + 0.14 n_E n_d^2\right) E_c d \qquad R^2 = 0.94$$

$$P_u(t) = \left(0.719 + 0.26 \times 0.98^t\right) \times 1.4\left(d^2 - d_s^2\right) f_{cd} + 1.2 d_s^2 f_{sd} \qquad R^2 = 0.94$$

$$S_p(t) = 2.71 - 0.62 \times 0.94^t \qquad R^2 = 0.94$$

$$S_u(t) = 0.000587t^2 - 0.08t + 8.39 \qquad R^2 = 0.95$$

Fig. 13 and Fig. 14 shows the fitting curves of $S_p(t)$ and $S_u(t)$ with different corrosion times.

The comparison of theoretical and test curves is shown in Fig. 15.

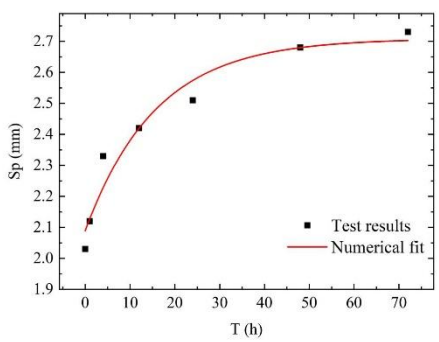

Fig. 13 Fitting curve of peak slip

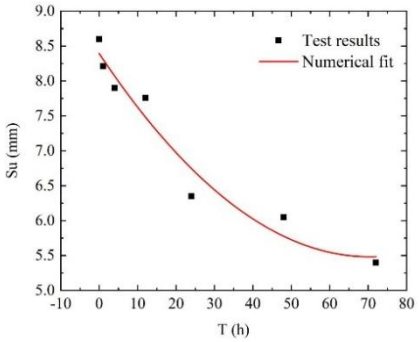

Fig. 14 Fitting curve of limit slip

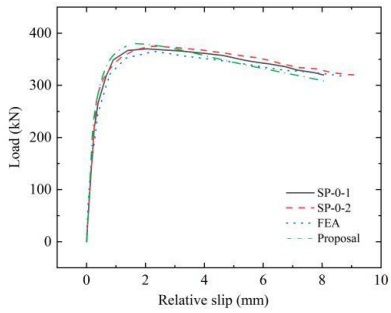

(a) 0 h

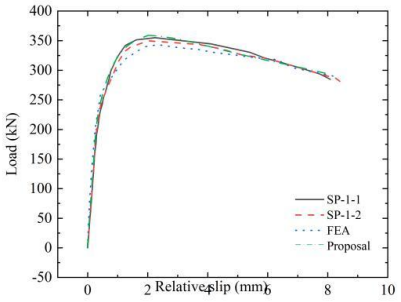

(b) 1 h

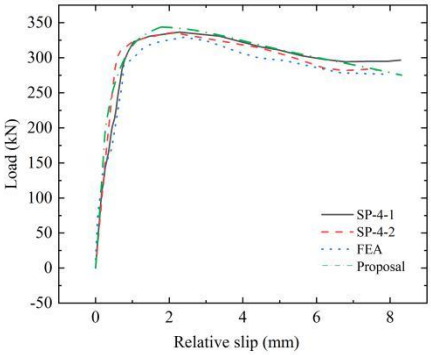

(c) 4 h

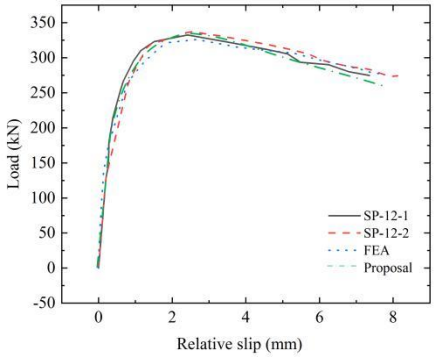

(d) 12 h

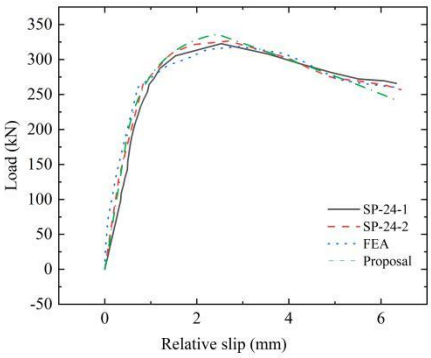

(f) 24 h

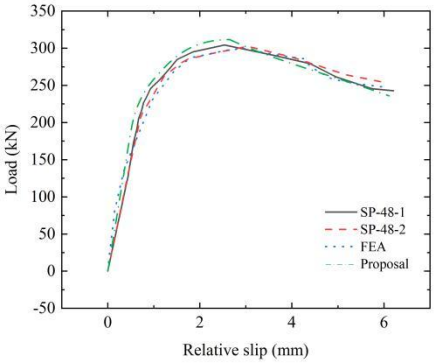

(g) 48 h

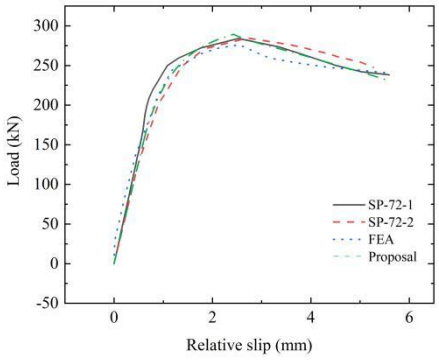

(h) 72 h

Fig. 15 Load-slip curve comparison for varying corrosion times

The consistency of the load-slip curve is evident, as the results from the formula calculation, testing, and finite element simulation match closely. Hence, formula (5) effectively represents the load-slip calculation model for PBL connectors subjected to hydrochloric acid corrosion.

6. Conclusions

Combined with the experimental research, theoretical analysis and finite element method, the following conclusions are drawn from 14 test specimens

and 147 finite element models.

(1) In push-out tests with varying corrosion times, the failure of shear link components is directly caused by the bending of steel bars and the cracking of concrete. After failure, the bending angle of the penetrated steel bar increases by 13.3°, while the cracking load and the load at the 45° inclined crack decrease by 74.9 kN and 81.3 kN, respectively.

(2) The load-slip curve of the PBL shear connector from 0 h to 72 h shows a 34.48% increase in the relative slip at maximum load, while the ultimate slip, shear stiffness, and ductility coefficient decrease by 59.25%, 8.22%, and 77.41%, respectively.

(3) An FEM model from 0 h to 72 h was established to compare with the test results. The slip decreased by 17.13% as the concrete strength increased from C30 to C60, and by 9.49% when the diameter of the penetrated steel bar increased from 12 mm to 25 mm. The slip under end pressure was reduced by 8.26% compared to non-end pressure, while an increase in the steel plate hole diameter from 35 mm to 65 mm led to an 11.77% reduction in slip.

(4) The failure modes of the shear link components are analyzed to understand their failure mechanism, and the load-slip curve is derived from the test data. The load-slip formula for the PBL shear connector corroded by hydrochloric acid is then developed based on the observed trends.

Author Contributions

Conceptualization, Yang, F.; methodology, Qiao, W.J.; software, Zhou, T.K.; writing—review and editing, Li, Y.L., Ruan, Z.D. and Li, S.F.. All authors have read and agreed to the published version of the manuscript.

Funding

This research was funded by the Natural Science Foundation of Shaanxi Province, grant number“ 2024JC-YBMS-427， 2024JC-YBMS-446”. This research was funded by the Natural Science Foundation of Shaanxi Province, grant number“ 2024SF-YBXM-618”.

Conflicts of Interest

The authors declare no conflict of interest.

References

[1] Zhan YL, ASCE M, Yin Chao, et al. Pushout Tests on Headed Studs and PBL Shear Connectors Considering External Pressure[J]. Journal of Bridge Engineering, 2020,25(1): 04019125.

[2] Kong FL, Huang PM, Han B, et al. Experimental Study on Behavior of Corrugated Steel-concrete Composite Bridge Decks with MCL Shape Composite Dowels[J]. Engineering Structures, 2021,227: 111399.

[3] Gu YW, Nie X, Liu YF, et al. Experimental and Numerical Study of Steel-to-concrete Joint Section in Hybrid Cable-stayed Bridges[J]. Journal of Constructional Steel Research, 2021,187, 106982.

[4] Hu WG, Zhang JL. Study on Static Lateral Load–slip Behavior of Single-shear Stapled Connections in Plywood for Upholstered Furniture Frame Construction[J]. Journal of Wood Science, 2021, 67:40.

[5] Zhang QH, Jia DL, Bao Y, et al. Internal Force Transfer Effect-based Fatigue Damage Evaluation for PBL Shear Connector Groups[J]. Journal of Constructional Steel Research, 2018, 148: 469-478.

[6] Wang BING, LIU Xiaoling, YI Xiyan.Load-slip calculation model of bolted connection under fatigue load.Journal of Harbin Institute of Technology, 2023,55 (11): 91-98.

[7] Yan LB, Han B, Fan L, et al. Fatigue Damage of PBH Shear Connector of Steel-concrete Composite Structure[J]. Engineering Structures, 2020,213: 110540.

[8] Xiao L, Qiang SZ, Xu X. Experimental Research on PBL Shear Connector for Steel-Concrete Composite Structures[J]. Advanced Materials Research, 2010, 163-167: 2137-2141.

[9] Aguiar OP, Caldas RB. Circular Openings with Transverse Rebar as Steel-concrete Shear Connection (part 1/2): Analytical model for strength and slip capacity[J]. Engineering Failure Analysis, 2022,133: 106007.

[10] Le N D ,Pham H T ,Pham D T , et al. An efficient long short-term memory-based model for prediction of the load-displacement curve of concrete-filled double-skin steel tubular columns [J]. Construction and Building Materials, 2024, 449 138122-138122.

[11] Tan XY, Fang Z, Xiong XW. Experimental Study on Group Effect of Perfobond Strip Connectors Encased in UHPC[J]. Engineering Structures, 2022,250: 113424.

[12] Zhao Y ,Song C ,Jinglai S , et al. Bar load-displacement curve model based on statistical damage mechanics [J]. Frontiers in Earth Science, 2022, 10

[13] Hao M ,Wei W ,Rongqiao X . Analytical model for the Load-Slip behavior of headed stud shear connectors [J]. Engineering Structures, 2022, 252

[14] Li SQ, Su LC, Sun ZB. Research on the Load-slip Properties of Corrugated Rib Connectors' Push-out Test[J]. KSCE Journal of Civil Engineering, 2018, 22(4), 12205.

[15] Wang WA, Zhao CZ, Li Q, Zhuang WL. Study on Load-Slip Characteristic Curves of Perfobond Shear Connectors in Hrbid Structures[J]. Journal of Advanced Concrete Technology, 2014, 12: 413-424.

[16] Cao JX, Liu YY, Wang YX, et al. Load-slip Performance of Timber-to-concrete Connections with U-steel Connectors under Push-out test[J]. Journal of Building Engineering, 2022, 45, 103527.

[17] Huang PM, He JL, Kong FL, et al. Experimental Study on the Bearing Capacity of PZ Shape Composite Dowel Shear Connectors with Elliptical Holes[J]. Scientific Reports, 2022, 12(1):2457.

[18] Gao YM, Li CJ, Wang XF, et al. Shear-slip Behaviour of Prefabricated Composite Shear Stud Connectors in Composite Bridges[J]. Engineering Structures, 2021,240: 112148.

[19] Li ZX, Zhao CH, Deng KL, et al. Load Sharing and Slip Distribution in Multiple Holes of a Perfobond Rib Shear Connector[J]. Journal of Structural Engineering, 2018, 144(9): 04018147.

[20] Zhang J, Hu XM, Kou LY, et al. Experimental Study of the Short-term and Long-term Behavior of Perfobond Connectors[J]. Journal of Constructional Steel Research, 2018, 150: 462-474.

[21] Yu ZL, Zhu B, Dou ST, et al. 3D FEM Simulation Analysis for PBL Shear Connectors[J]. Applied Mechanics and Materials, 2012,170-173:3449-3453.

[22] Tan XY, Fang Z, Xiong XW. Experimental Study on Group Effect of Perfobond Strip Connectors Encased in UHPC[J]. Engineering Structures, 2022,250: 113424.

[23] Jiang HB, Fang HZ, Liu J, Fang ZC, Zhang JF. Experimental Investigation on Shear Performance of Transverse Angle Shear Connectors[J]. Structures, 2021, 33:2050-2060.

[24] GB/T 228.1-2021, Metallic Materials-Tensile Testing-Part 1: Method of Test at Room Temperature, Chinese Standard, 2021.